IOPscience iopscience.iop.org

Home Search Collections Journals About Contact us My IOPscience

Microchannel neural interface manufacture by stacking silicone and metal foil laminae

This content has been downloaded from IOPscience. Please scroll down to see the full text.

2016 J. Neural Eng. 13 034001

(http://iopscience.iop.org/1741-2552/13/3/034001)

View the table of contents for this issue, or go to the journal homepage for more

Download details:

IP Address: 128.40.160.220
This content was downloaded on 04/04/2016 at 11:48

Please note that terms and conditions apply.

OPEN ACCESS
IOP Publishing
Journal of Neural Engineering
J. Neural Eng. 13 (2016) 034001 (9pp)
doi:10.1088/1741-2560/13/3/034001

Note

# Microchannel neural interface manufacture by stacking silicone and metal foil laminae

**Henry T Lancashire[1], Anne Vanhoestenberghe[2,3], Catherine J Pendegrass[1], Yazan Al Ajam[1], Elliot Magee[2,3], Nick Donaldson[3] and Gordon W Blunn[1]**

[1] University College London, John Scales Centre for Biomedical Engineering, Institute of Orthopaedics and Musculoskeletal Science, RNOHT, Stanmore HA7 4LP, UK
[2] University College London, Centre for Rehabilitation Engineering and Assistive Technology, Institute of Orthopaedics and Musculoskeletal Science, RNOHT, Stanmore HA7 4LP, UK
[3] University College London, Implanted Devices Group, Department of Medical Physics and Biomedical Engineering, Malet Place Engineering Building, Gower Street, London WC1E 6BT, UK

E-mail: henry.lancashire.10@ucl.ac.uk

Received 15 June 2015, revised 14 November 2015
Accepted for publication 15 February 2016
Published 22 March 2016

**Abstract**

*Objective.* Microchannel neural interfaces (MNIs) overcome problems with recording from peripheral nerves by amplifying signals independent of node of Ranvier position. Selective recording and stimulation using an MNI requires good insulation between microchannels and a high electrode density. We propose that stacking microchannel laminae will improve selectivity over single layer MNI designs due to the increase in electrode number and an improvement in microchannel sealing. *Approach.* This paper describes a manufacturing method for creating MNIs which overcomes limitations on electrode connectivity and microchannel sealing. Laser cut silicone—metal foil laminae were stacked using plasma bonding to create an array of microchannels containing tripolar electrodes. Electrodes were DC etched and electrode impedance and cyclic voltammetry were tested. *Main results.* MNIs with 100 $\mu$m and 200 $\mu$m diameter microchannels were manufactured. High electrode density MNIs are achievable with electrodes present in every microchannel. Electrode impedances of 27.2 $\pm$ 19.8 k$\Omega$ at 1 kHz were achieved. Following two months of implantation in Lewis rat sciatic nerve, micro-fascicles were observed regenerating through the MNI microchannels. *Significance.* Selective MNIs with the peripheral nervous system may allow upper limb amputees to control prostheses intuitively.

S Online supplementary data available from stacks.iop.org/JNE/13/034001/mmedia

Keywords: micromachining, neural interfaces, microchannels, laser cutting

(Some figures may appear in colour only in the online journal)

## Introduction

Recording and stimulating neural activity with high selectivity has the potential to enable upper limb amputees to control prostheses intuitively [1]. However recording extracellularly from peripheral nerves presents a challenge: action currents are small and (for myelinated axons) are concentrated

Original content from this work may be used under the terms of the Creative Commons Attribution 3.0 licence. Any further distribution of this work must maintain attribution to the author(s) and the title of the work, journal citation and DOI.

 © 2016 IOP Publishing Ltd Printed in the UK

at small, regularly spaced unmyelinated sections in the nodes of Ranvier [2]. In addition, nerves are surrounded by muscles producing relatively large myoelectric potentials (EMG) that interfere with the neural signals.

Microchannel neural interfaces (MNIs) have been developed to overcome issues with recording axonal action potentials [2–5]. MNIs are regenerative neural interfaces with an array of microchannels into which peripheral nerves regenerate. By confining the axons within a long, small diameter electrically insulating channel the signal amplitude is increased, cross-talk is reduced and recordings can be made independent of node of Ranvier position. MNIs have been manufactured by block casting silicone around removable filaments [3, 5, 6], polyimide thin-film processes have made interfaces which can be rolled [3, 4, 7], or capped with polydimethylsiloxane film (PDMS, a silicone) [8, 9]. Photopatternable silicone has been used in place of polyimide to reduce interface stiffness [10] and plasma bonding has been used to add SU-8 cast microchannel caps to thin-film silicone interfaces [11, 12]. Designs have been developed where the microchannels are sealed with a lid during surgery [13].

Problems with microchannel sealing in rolled polyimide MNIs have been reported, which reduced the insulation between adjacent microchannels, decreasing selectivity [3]. A complete bond between the microchannel sidewalls, base, and lid sections is essential. In addition, rolled and other single layer MNIs limit electrode number: tracks and interconnects take up lateral space on the implant reducing the number of available electrodes. Rolled polyimide interface designs have electrodes present in less than 10% of microchannels [3, 7]. Stacking multiple microchannel layers, rather than rolling a single microchannel layer may help overcome these limitations, allowing the manufacture of MNIs with a higher density of electrode sites suitable for long term implantation [12].

To date MNI designs have focussed on tripolar electrode arrangements [3, 11], however alternative electrode arrangements are under investigation [6, 14, 15]. This work will use tripolar configurations because the efficacy of these electrodes has been demonstrated in MNIs [16].

Schuettler *et al* have used laser cutting of spin coated silicone rubber and platinum foil to form implantable microelectrode arrays [17]. This process uses thin metal foil instead of sputter deposited metallisation, creating thicker metal tracks with reduced flexibility but greater robustness. The metal foils are typically 12.5 $\mu$m thick, however 5–25 $\mu$m foils can be used to change flexibility or stability. This technique has been expanded to form multi layered devices whereby more electrodes can be included (around 4.5 $mm^{-2}$) by vertically separating electrode tracks [18] and can be used to create devices with microfluidic channels [19, 20].

In this note we demonstrate a manufacturing method for creating MNIs that overcomes limitations on electrode number and microchannel sealing. The method described uses microchannel laminae of laser cut silicone rubber and metal foil, which are then plasma bonded to form a stacked microchannel array. In order to demonstrate their utility, a brief description of short term *in vivo* results obtained using these new MNIs is given.

## Materials and methods

### *Equipment and materials*

The methods presented are based on work by Schuettler *et al* [17], however there are key differences in the equipment used.

Laser cutting was carried out using an Nd:YAG laser (Laserval Violino-2, laser system by Laser Lines Ltd, UK), with a wavelength of 1064 nm, pulse width of 12 ns, pulse energy up to 500 $\mu$J, and repetition rate up to 10 kHz. A spot size of 30 $\mu$m was achieved, limiting the minimum feature size. A high speed scan head (up to 7000 mm $s^{-1}$) was used to guide the laser spot within a 60 mm × 60 mm flat field. An aluminium peg-board with sprung pins was used to hold glass slides in place within the field. High-efficiency particulate arrestance (HEPA) filtered airflow was used to cool the sample and remove vapour, dust and sputtered metal during laser cutting. Laservall Smartist 4.1 software on Windows XP was used to control the laser system.

Spin coating was carried out using a custom polytetrafluoroethylene (PTFE) holder in a WS-400E-NPP-Lite spin coater (Laurell Technologies). Standard glass microscope slides (75 mm × 25 mm, 1 mm thick) were used as carriers for lamina manufacture. A release layer of polystyrene sulfonic acid (PSS, 561223 Sigma, UK) was spin coated onto the glass slides at 2000 rpm for 10 s, then baked at 80 °C for 15 min. When placed in distilled water the PSS layer swells and samples can easily be removed from the glass slide.

Two-part silicone (PDMS, Sylgard 184, Dow Corning) was used as a structural material and an insulator. The silicone was prepared at a 10 to 1 mix ratio and 0.25 parts black pigment (Med-4800-2, Polymer Systems Technology Limited) was added. Silicone was mixed using a Speedmixer for 2 min at 2500 rpm (Dual Asymmetric Centrifugal Laboratory Mixer System, DAC 150 FVZ-K, Synergy Devices Ltd). Silicone was degassed at 30 mbar in a vacuum centrifuge for between 1 and 3 min, until bubbles were no longer visible.

In this paper 12.5 $\mu$m stainless steel foil was used (Advent Research Materials, UK). Prototyping was carried out using aluminium foil (kitchen grade, various suppliers). Before use the foil was cut to size using the laser cutter and cleaned with isopropyl alcohol.

Plasma bonding was carried out using a plasma chemistry unit (Plasmaprep 100, Nanotech Ltd). Silicone surfaces for bonding were cleaned with isopropyl alcohol and air-dried. Silicone surfaces were plasma treated using air plasma for 2 min at 2 Torr, forward power was 50 W and reflected power was 10 W. Samples were removed from the plasma chemistry unit, aligned under a light microscope, and bonded by applying pressure within 2 min. Pressure was applied using a modified G-clamp to deform the surfaces and ensure adhesion across the entire sample. Following alignment, clamped samples were placed in an oven at 80 °C for at least 1 h to bond.

### *Implant fabrication*

The MNIs were formed of identical microchannel laminae, which were then plasma bonded. Each lamina was formed

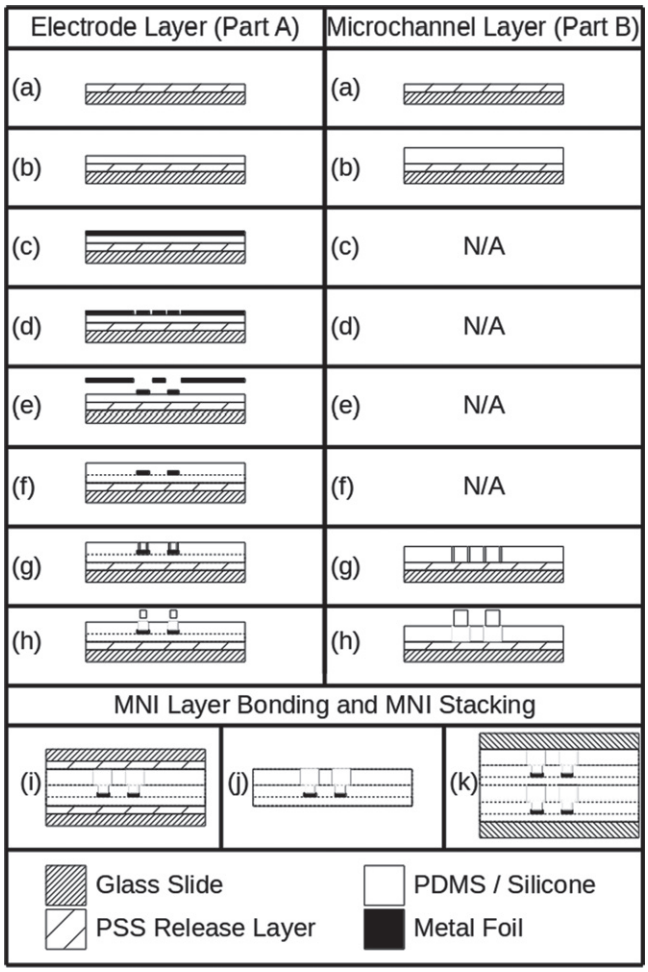


**Figure 1.** An overview of microchannel neural interface manufacture by stacking and plasma bonding. Part A and Part B manufacture (a)–(h) and stacking (i)–(k) are described. (a) PSS spin coated onto glass slide. (b) PDMS spin coated. (c) Metal foil placed on PDMS. (d) Metal foil laser cut. (e) Excess metal foil removed. (f) Second PDMS layer spin coated. (g) PDMS layer laser cut. (h) Excess PDMS removed. (i) Parts A and B plasma bonded. (j) PSS removed in water bath leaving a complete microchannel lamina. (k) Microchannel laminae are plasma bonded and stacked between PTFE supports. Part A and Part B manufacture (a)–(h) modified from [17], © IOP Publishing. Reproduced with permission. All rights reserved.

from two parts joined by plasma bonding. The two parts will be referred to as the electrode layer (Part A), and the microchannel layer (Part B).

The processes for forming Parts A and B are summarised in figures 1(a)–(h) and details are given in table 1. Micrographs for key process stages are presented in figures 2(a)–(h). PDMS was spin coated onto PSS coated glass slides and cured in an oven (figures 1(a)–(b) and table 1(a)–(b)). For Part A, metal foil was carefully placed onto the silicone avoiding air bubble formation and smoothed using a lint free cloth soaked in isopropyl alcohol (figure 1(c) and table 1(c)). For Part A, tracks and pads were patterned by laser cutting the metal foil and removing the excess using tweezers (figures 1(d)–(e) and table 1(d)–(e)). A second layer of silicone was spin coated onto the patterned foil at 1000 rpm for 45 s and cured in an oven (figure 1(f) and table 1(f)). Electrode pads (Part A) and microchannels (Part B) were patterned by laser cutting the silicone (figure 1(g) and table 1(g)) and removing the excess using tweezers. Cut silicone was cleaned with a lint free cloth soaked in isopropyl alcohol, this helped lift the cut silicone strips. Finally Parts A and B were completely cured in an oven (figure 1(h) and table 1(h)).

Parts A and B were plasma bonded to form a single MNI lamina. Before bonding excess silicone surrounding the patterned metal and microchannel areas was removed to within 5 mm of the area of interest. The MNI lamina was released from the carrier in de-ionised water (figures 1(i)–(j)).

MNI laminae were bonded to form a stacked MNI (figure 1(k)). PTFE slides were used as carriers to prevent unwanted bonding. Stacks were bonded such that Part A of one lamina sealed the microchannels of the lamina below. Stacking and bonding was repeated until a suitably sized interface was made. Microchannels in the uppermost MNI lamina were sealed by plasma bonding a spin coated, PDMS layer. (We use *sealed* to mean that ionic current can only flow from electrodes in the microchannel out at the ends of the lumen.)

Parts A with and without metal foil can be used to create active or passive laminae. By staggering pad placement on Parts A access to pads on many laminae can be achieved [18], alternatively Parts A can be bonded back-to-back allowing access to pads from opposite faces of the MNI.

Silicone tubing (SFM3-2350, Polymer Systems Technology Limited) was used to enclose the neural interfaces and provide a surface for suture attachment to the peripheral nerve epineurium. Tubing was attached to the neural interface using a silicone adhesive (3140 RTV, Dow Corning) and cured at 60 °C for at least 12 h. Prior to *in vivo* use implants were cleaned in 70% ethanol and autoclaved at 121 °C for 15 min. Sterile implants were stored in sterile isotonic saline.

### *Impedance reduction, spectroscopy and cyclic voltammetry*

To reduce electrode impedance, all electrodes were direct current (DC) etched by applying +4 V DC relative to a large (>4 $cm^2$) indifferent electrode in fresh 0.9% saline for 5 min. Impedance of all electrodes was measured before and after DC etching, impedance was measured between one interface electrode and a large (>4 $cm^2$) electrode. Cyclic voltammetry (CV) was carried out before and after DC etching to determine electrode charge storage capacities (CSC).

To determine channel sealing, electrode impedance was measured between single interface electrodes and a large (>4 $cm^2$) electrode. Fully-sealed and partially-sealed microchannels ($n = 6$) were identified by light microscopy (see supplementary materials). Electrode impedance was measured from the open-ended (as produced) MNI. The ends of the electrode-containing microchannel were blocked with petroleum jelly (Vaseline, Unilever, UK) leaving other microchannels open-ended. Electrode impedance was re-measured and fully-sealed and partially-sealed microchannels were compared.

**Table 1.** Details of processing steps for Parts A and B. There are key differences in parameters between each process.

| Processing step | Electrode layer (Part A) | Microchannel layer (Part B) |
|---|---|---|
| (a) Spin coat PSS | 2000 rpm for 10 s | 2000 rpm for 10 s |
| (b) Spin coat and cure silicone | 1000 rpm for 45 s, 60 °C for 1 h (part cure) | 500 rpm for 45 s, 100°C for 1 h |
| (c) Foil | Yes | N/A |
| (d) Laser cut foil | Yes | N/A |
| (e) Remove excess foil | Yes | N/A |
| (f) Spin coat and cure Silicone | 1000 rpm for 45 s, 100 °C for 1 h | N/A |
| (g) Laser cut silicone | Yes | Yes |
| (h) Remove excess silicone and cure | Yes, 100 °C for at least 1 h | Yes, 100 °C for at least 1 h |

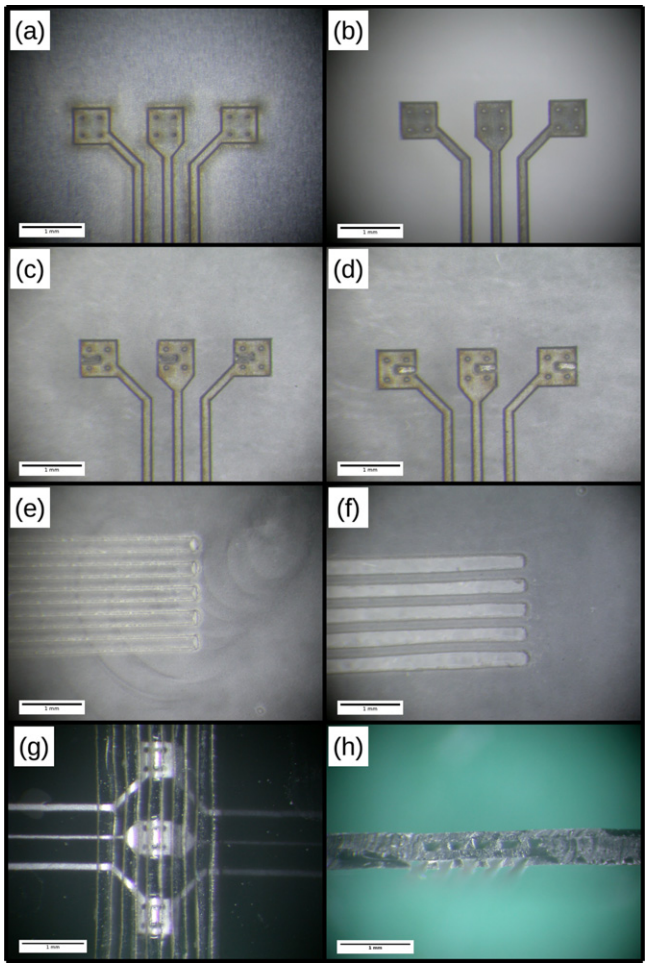


**Figure 2.** Light micrographs showing microchannel neural interface manufacture by stacking and plasma bonding. Part A and Part B manufacture (a)–(f) and stacking (g), (h) are shown. (a) Metal foil laser cut. (b) Excess metal foil removed. (c) Second PDMS layer spin coated and laser cut. (d) Excess PDMS removed exposing electrodes. Part B manufacture (e)–(f): (e) PDMS layer spin coated and laser cut. (f) Excess PDMS removed leaving microchannels. (g) Parts A and B plasma bonded (top view). (h) Two stacked microchannel laminae (end view). Slight misalignments are present in c and d. All scale bars = 1 mm.

Crosscut sprung pin probes (RS Components, UK) were used to form an electrical connection with the pads. Before connection a stiff layer was placed underneath the MNI, e.g. a ruler or a glass slide, and the pin probes were pressed gently into contact with the pads.

To measure electrode impedance MNIs were placed in fresh 0.9% saline and the saline was degassed under vacuum at 25 mbar for 5 min. *In vitro* impedance measurements were made using a Wayne-Kerr 6500B Precision Impedance Analyser (Wayne Kerr Electronics, UK, 20 Hz–1 MHz, 50 mV excitation voltage).

To measure electrode CSC, MNIs were placed in phosphate buffered saline purged with $N_2$. Following 30 mins settling time CV measurements were made using a ModulabXM Potentiostat (Solartron Analytical, USA), with a sweep rate of 50 mV $s^{-1}$ from −0.6 V to +0.8 V (the empirically determined water window). A saturated calomel electrode (SCE) reference electrode and a platinum counter electrode were used. Data was recorded using ModulabXM ECS software (version 2.2.x, Solartron Analytical) and plotted using CView software (version 3.4b, Scribner Associates Inc., USA).

### *Vertical scanning interferometry (VSI)*

Microchannels (Part B) and metal electrode surfaces were examined using VSI. Samples were placed in an interferometer (Contour GT, Bruker) and images were recorded using Vision64 software (Release v5.30, Bruker). Vertical travel was adjusted depending upon sample profile. Microchannels were imaged at 5×, 10×, and 20× magnification.

### *Implantation*

All *in vivo* procedures were carried out in compliance with The Animals (Scientific Procedures) Act UK, 1986 (revised 2013) and local guidance. Sterile procedures were used throughout. Rats (12 week, male, Lewis) were anaesthetised with with 2% isoflurane (Isoflo, B506, Abbott) in oxygen (1–2 l $min^{-1}$). Animals were placed in the right lateral position. The operation site was shaved and prepared with Hydrex Clear (0.5% w/v chlorhexidine gluconated in 70% v/v denatured ethanol B, Ecolab Ltd) and the operative field draped. The left sciatic nerve was exposed and freed from surrounding tissue. The sciatic nerve was divided between the proximal and middle third of the thigh. The proximal nerve end was placed in the lumen of the implant abutted to the microchannels. The nerve was sutured to the implant using 9-0 polyamide monofilament suture (S&T, 03180, Interfocus Ltd, UK). Three epineurial sutures were used equidistant around the nerve. Sutures were passed through the

perineurium proximally to distally and through the wall of the silastic tubing before being secured. The implant was manipulated to access the reverse side for suturing. The distal end was sutured in the same manner with sutures passing through the perineurium distally to proximally and through the wall of the silastic tubing. The incision was closed with a continuous buried subcuticular suture using 4-0 polyglactin 910 sutures (Vicryl, W9106, Johnson & Johnson International, UK). The wound was treated with moisture permeable spray dressing (Opsite, Smith and Nephew). Analgesia was performed immediately postoperatively using 3 $\mu$g buprenorphine subcutaneously (as buprenorphine hydrochloride, 3.24 $\mu$g in 1 ml, Vetergesic, Sogeval UK Ltd). Animals were returned to darkened group housing and monitored until recovery from anaesthesia was confirmed. A total of 24 animals were implanted with MNIs. Animals were housed in groups of 4.

### *Histology*

A modified nerve fixation method was used [21]. Animals were sacrificed by cervical fracture after one month and two months post-operatively. The neural interface and 1 cm of distal and proximal nerve were excised and immediately fixed with 4% paraformaldehyde buffered saline. The nerves were washed and stored at 4 °C in 0.2% glycine in buffered saline. The distal and proximal nerve sections were identified and removed carefully to preserve micro-fascicles in continuity with the distal end. Samples were post-fixed for 2 h in 1% osmium tetroxide (Agar Scientific, UK) in 0.1 M sodium cacodylate buffer. Samples were dehydrated in ascending alcohol series, embedded in paraffin, and 5 $\mu$m transverse sections were taken using a rotary microtome. Sections were stained with Harris Haemotoxylin (Sigma HHS32) and Eosin (eosin Y-solution, 0.5% aqueous, Merck KGaA, 1.09844.1000), mounted with DPX mountant (VWR, 360294H), and were imaged using an Axioskop 2 Plus light microscope (Zeiss) with Axiovision software (Zeiss).

### *Statistical analysis*

Statistical analyses were carried out using SPSS Statistics 22 (IBM). Data are reported as mean ± standard deviation to three significant figures. Mann-Whitney U tests of significance were used for independent samples and Wilcoxon signed-rank tests were used for paired samples, significance was tested at the $\alpha = 0.05$ level.

## Results

MNIs were manufactured using the stacking method (figures 2(a)–(h) and 3(a)–(d)). Microchannel laminae with electrodes present in all microchannels have been demonstrated (figure 3(d)), these can be used in microchannel stacks to create well connected active implants. Up to 6 microchannel laminae have been stacked, however due to the dimensions of rat sciatic nerve only 4 laminae were used in practice (figure 3(b)). For rat sciatic nerve prototypes one microchannel per lamina was connected with a tripolar electrode configuration, providing 3 electrode sites per lamina, or 12 electrode sites in a 4 laminae structure.

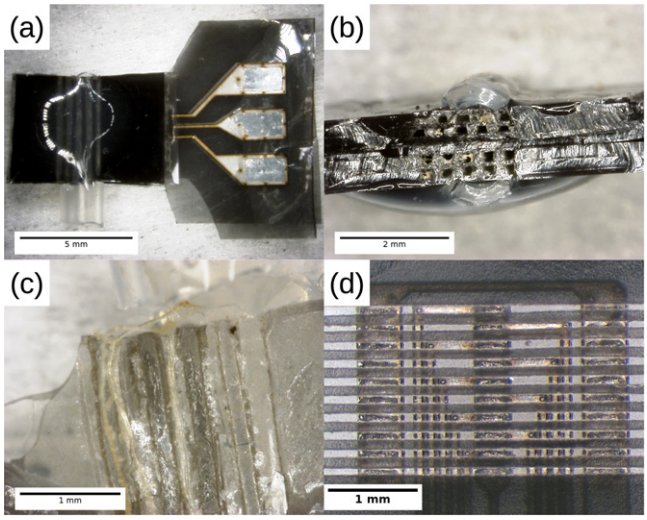


**Figure 3.** Microchannel neural implant following two months nerve regeneration (a)–(c), and a high electrode density MNI layer (d). (a) Complete implant with silicone tubing removed from one side (scale bar = 5 mm). (b) End view of microchannels with some adherent tissue present. Four stacked layers are visible (scale bar = 2 mm). (c) Microfascicles regrown through microchannels (scale bar = 1 mm). (d) An increased number of electrode sites in a single microchannel lamina (scale bar = 1 mm). A sketch detailing the images is available in supplementary materials, figure S1(a)–(d).

Microchannel dimensions in part B were determined using VSI (figure 4(a)) and light microscopy (figures 2(g), (h) and 3(b)). 200 $\mu$m diameter channels were chosen because at this width the PDMS could be reliably cut using the laser without causing the separating ridges to fail. Figure 4(a) shows that channel walls are uniform at 150 $\mu$m cutting depth. The microchannels shown in figure 3(b) are 200 $\mu$m × 150 $\mu$m cross section, with a pitch of 400 $\mu$m horizontally and 250 $\mu$m vertically, MNIs with these dimensions were used in this work. Once stacked the microchannels have a trapezoid cross section (figures 2(h) and 3(b)), this is created partly by the laser (a wider heat affected zone is present at the silicone surface) and partly by deformation due to the pressure applied during plasma bonding. The laser cut silicone side walls are rough (3.07 ± 0.551 $\mu$m $R_a$, $n = 6$) compared with the uncut silicone forming the channel lid and base (0.0642 ± 0.0176 nm $R_a$, $n = 6$). Microchannel dimensions can be varied, microchannels with 100 $\mu$m × 100 $\mu$m cross section are shown in figure 3(d), and VSI of similar microchannels is shown in figure S4. This improvement in microchannel pitch, to 200 $\mu$m, allows for ten channels containing electrodes within 2 mm, and makes much higher electrode densities possible.

Electrode impedance at 1 kHz was significantly lower after DC etching (27.2 ± 19.8 kΩ) than before (88.9 ± 66.9 kΩ, $p < 0.001$), see figure 4(b). Electrode surface roughness was significantly greater following DC

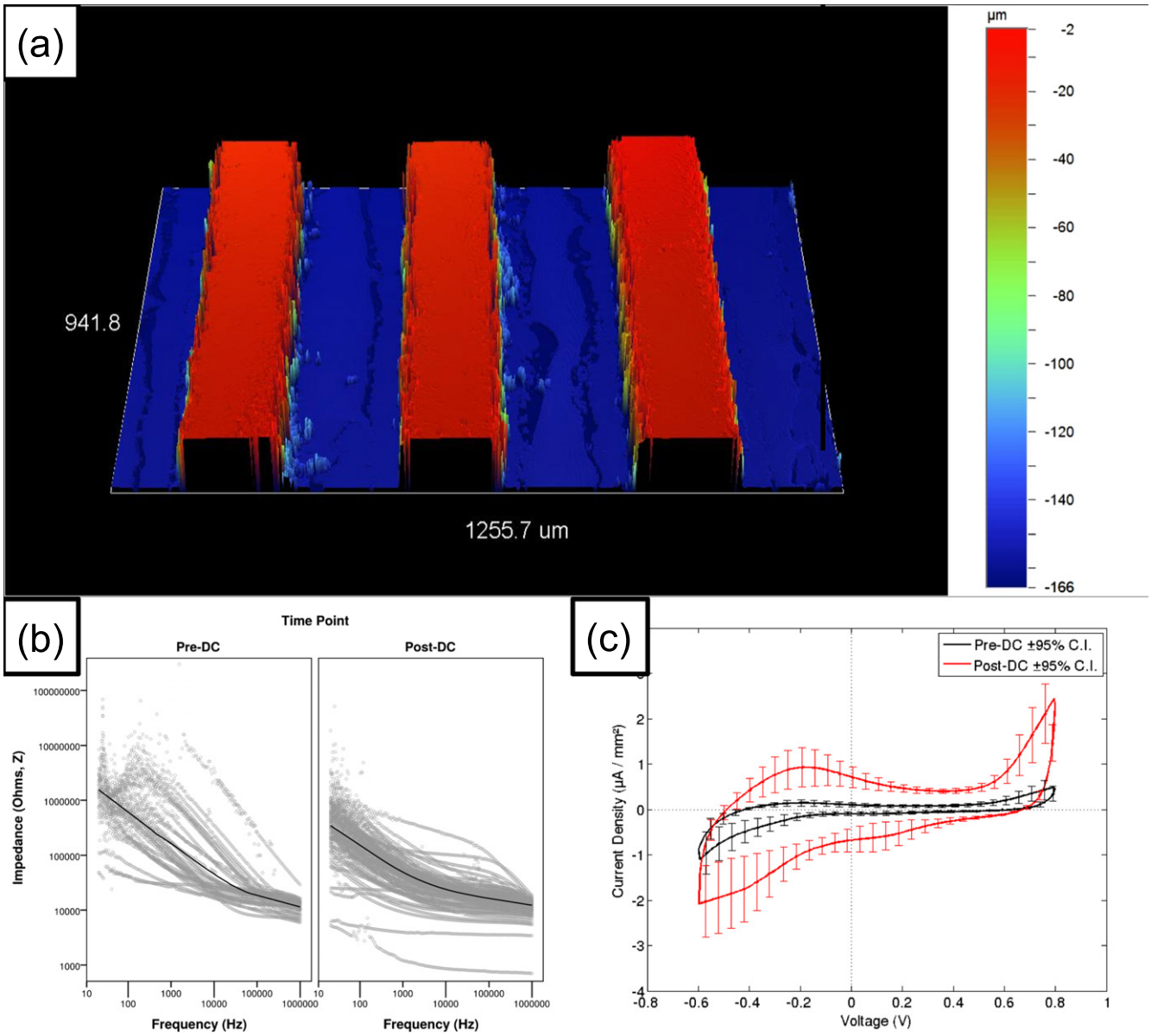


**Figure 4.** Characterisation of microchannel neural interfaces. (a) Vertical scanning interferometry image of Part B, the laser cut silicone microchannels. (10× magnification). Microchannels are 150 $\mu$m depth, 200 $\mu$m width, separated by 200 $\mu$m wide silicone strips. (b) Impedance Spectrographs of microchannel neural interface electrode impedance before and after etching with +4V DC current ($n = 24$, grey points). Plotted on a log–log scale with a local regression fit (black line). (c) Cyclic Voltammetry at 50 mV $s^{-1}$ of stainless steel electrodes before and after etching with a +4V DC current. Mean current density normalised to geometric electrode area with 95% confidence intervals ($n = 6$ samples per group, 10 sweeps averaged per sample). Voltage versus SCE in PBS.

etching: from $0.248 \pm 0.0579\,\mu$m $R_a$ pre-etching to $0.575 \pm 0.483\,\mu$m $R_a$ post-etching ($p = 0.009$). Electrode CSC and CV response to a 50 mV $s^{-1}$ sweep changed following DC etching. CV response is shown in figure 4(c). CSC was significantly lower before DC etching ($0.716 \pm 0.372$ mC $cm^{-2}$) than after ($3.72 \pm 1.42$ mC $cm^{-2}$, $p = 0.031$, $n = 6$). Cathodic CSC was also significantly lower before DC etching ($0.414 \pm 0.222$ mC $cm^{-2}$) than after ($1.92 \pm 0.793$ mC $cm^{-2}$, $p = 0.031$, $n = 6$).

The effectiveness of plasma treatment in forming complete bonds between the side walls, lid and base, to seal the microchannel, was tested. Both ends of a single microchannel were blocked with petroleum jelly, and the impedance with respect to an electrode outside the microchannel was measured. Where microchannels were completely sealed and channel ends were blocked, electrode impedance readings ($41.2 \pm 24.6$ MΩ) were not significantly different from open-circuits, formed by disconnecting the counter electrode from the impedance analyser ($56.6 \pm 38.0$ MΩ, $p = 0.553$). Where the channel ends were blocked but the plasma bonds were incomplete creating an incompletely sealed microchannel, electrode impedance ($30.8 \pm 4.29$ kΩ) was not significantly different from electrodes in open ended microchannels ($27.2 \pm 19.8$ kΩ, $p = 0.884$), and was significantly lower than for electrodes in completely sealed microchannels ($p < 0.001$). The completeness of the seal was confirmed using light microscopy. This is shown in supplementary figures S2 and S3.

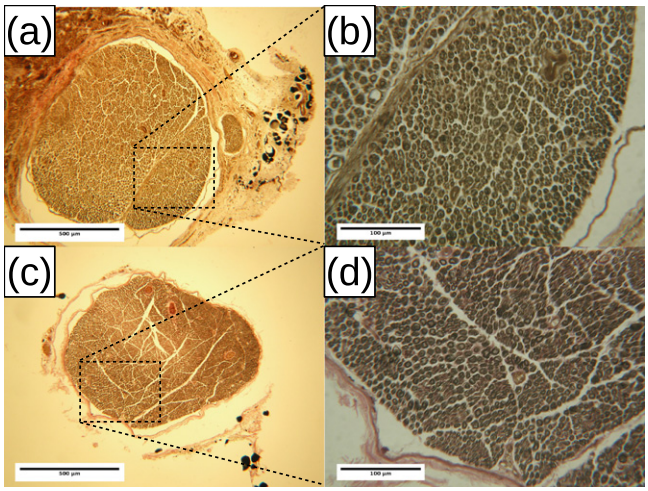


**Figure 5.** Transverse histological sections of proximal (a), (b) and distal (c), (d) nerve following regeneration through a microchannel neural interface. (a), (c) at 10× magnification showing the whole nerve with 500 $\mu$m scale bars, (b), (d) at 40× magnification showing myelinated axon detail (dense ring structures) with 100 $\mu$m scale bars.

Two months post-operatively micro-fascicles could be seen within the microchannels (figures 3(b) and (c)). The distal nerve regenerated and myelinated axons could be observed (figures 5(a)–(d)). Sectioning through the implant was not possible, and as previously noted by other groups [12], sectioning of microfascicles was difficult, therefore sections proximal and distal to the implant are reported.

## Discussion and conclusion

The goal of this study was to manufacture high electrode density MNIs using silicone—metal foil laminates which are stacked using plasma bonding to form an array of microchannels. 200 $\mu$m and 100 $\mu$m wide microchannels were formed with electrodes present in up to 100% of microchannels. Limits on size are imposed by the laser spot size (30 $\mu$m) [17], but might be reduced to less than 15 $\mu$m using 10 ps laser pulses [22]. The pressure applied during plasma bonding enabled the microchannels to be well sealed and any unsealed sections could immediately be seen under light microscopy and rejected, the difference between sealed and unsealed microchannels was demonstrated using impedance spectroscopy. Wall dimensions are key to microchannel sealing, 200 $\mu$m wide PDMS walls were used for the majority of this study; however, 100 $\mu$m wide walls have been shown (figure 3(d)), with increased electrode density. Other work has demonstrated further reductions in wall width, plasma bonding 50 $\mu$m wide PDMS walls [12].

This work used a 1064 nm laser to cut both the metal foil and PDMS. Previous work has used a frequency doubling crystal and a 1064 nm laser to achieve a wavelength of 532 nm [17], which allows cutting of unmodified silicone, while in this work black pigment was used. The addition of black pigment to the PDMS was key to accurately laser cutting PDMS to a depth greater than 50 $\mu$m using the 1064 nm laser. The cut silicone side walls exhibit micron-scale roughness which may influence neural regeneration. Isotropic roughened surfaces alter neuronal response *in vitro*, though the *in vivo* neural regeneration response to roughened surfaces is not yet clear [23]. In our *in vivo* study nerve regeneration was observed, indicating that this roughness is not a consequential inhibitor of neural regeneration.

Our work used Sylgard 184 PDMS, an industrial silicone commonly used for MNI micromanufacture [5, 10, 11, 13]. For clinical applications a medical grade silicone should be chosen (e.g. MED-1000, MED-2000), these have been used previously in laser cut silicone—metal foil laminates [17]. In addition, the relative stiffness of the implant and the nerve are important. The modulus of elasticity of peripheral nerve varies with species and tissue, values from 10 MPa to $<$1 MPa are reported [24]. Silicone elastic modulus falls in this range [25, 26], therefore the mismatch with the bulk MNI material is minimised. However, stainless steel and platinum foils are much stiffer (170–200 GPa). Evaporated metal tracks can be used as a flexible alternative [12]. Interface transparency (% open cross-sectional area) can be increased by thinning the microchannel side-walls and the electrode layer (part A). By spin coating at higher speeds silicone thickness can be reduced, alternatively uncured silicones can be mixed with *n*-heptane to reduce viscosity [17]. Transparency of the implanted interface was 28% (figure 3(b)), this has been increased to 35% by spin coating at higher speeds (supplementary figure S2(a)). This is greater than previous silicone implants (21%), but ideally should be increased to at least the levels achieved in polyimide designs (62%) [3].

The DC etching method presented in this paper lowered electrode impedances and increased electrode surface roughness and charge storage capacity. Stainless steel (316L) is an accepted implantable material, this modification may alter the biocompatibility of the electrode material. Previous *in vitro* data suggest that biocompatibility is not impaired by electropolishing of stainless steel [27]; however, DC etching should be investigated. The CSC and cathodic CSC of the etched electrodes approaches values achieved with smooth platinum electrodes, using roughened platinum foils instead of stainless steel can further increase the CSC of small electrodes [28, 29].

The human median and ulnar nerves have median diameters of approximately 5 mm proximal to the elbow [30]. This paper focussed on the development of interfaces for rat sciatic nerve of 1–1.5 mm diameter, therefore larger MNIs with a greater number of channels would be needed for human applications. The stacking method is well suited to producing large MNIs with many layers of active or passive microchannels, passive MNIs of up to 6 laminae have been prototyped. In the high electrode density designs 11 connections per lamina are made (10 recording electrodes and 1 common pseudotripolar reference in 100 $\mu$m wide channels, figure 3(d)), this introduces many more active channels. By stacking microchannel laminae with these properties 100 microchannels containing electrodes in a 2 mm × 2 mm cross section is achievable. This compares well with previous

studies showing MNI devices with 20 [3, 7], 10 [12], 8 [6, 9], 5 [13], and 4 [31] microchannels containing electrodes. It must be noted that the *in vivo* evaluation in this paper used larger microchannels (200 $\mu$m) with electrode present in two microchannels, and that neural regeneration is better through larger microchannels [5].

Electrical continuity with the contact pads remains a challenge. In the work presented here sprung pins on a 2 mm pitch were used to make temporary contact. Previous work with microchannels has used similar connection methods with needles [3]. Alternatively other research has used microwires which are introduced into the microchannels during manufacture [6, 9, 13], or *in vivo* [3, 13]. Conductive paste has been used to connect to soft thin-films [11]. These approaches are suitable for short term evaluation, but preferably for long term applications in animals a headstage would be used [6], avoiding the need for invasive surgery during recording, this will require an interconnect between the MNI and a printed circuit board, cable or application specific integrated circuit. Interconnects between soft thin-films or metal foils and stiff substrates have been achieved by micro-rivet bonding [7, 32, 33], parallel gap welding, laser welding, soldering [34] and plasma bonding to glass substrates with gold bumps [35]. An interconnect technology should be chosen for use with MNIs in long term *in vivo* evaluations.

Stacked MNIs have been successfully manufactured using laser cutting and plasma bonding. Nerve regeneration through the microchannels has been demonstrated following two months *in vivo*. Stacked MNIs overcome limitations on electrode number and microchannel sealing. We propose that the use of these new stacked MNIs will improve selectivity over single layer MNI designs due to the increase in electrode number and an improvement in microchannel sealing.

## Acknowledgments

HL would like to acknowledge Engineering and Physical Sciences Research Council, grant no EP/G036675/1 for financial support under their Centres for Doctoral Training scheme. G Hughes (Royal Veterinary College, UK), R Ferro de Godoy (UCL, UK) and A Mosse (UCL, UK) provided technical assistance and advice.

## References

[1] Dhillon G S and Horch K W 2005 Direct neural sensory feedback and control of a prosthetic arm *IEEE Trans. Neural Syst. Rehabil. Eng.* **13** 468–72

[2] Fitzgerald J J, Lacour S P, McMahon S B and Fawcett J W 2008 Microchannels as axonal amplifiers *IEEE Trans. Biomed. Eng.* **55** 1136–46

[3] FitzGerald J J, Lago N, Benmerah S, Serra J, Watling C P, Cameron R E, Tarte E, Lacour S P, McMahon S B and Fawcett J W 2012 A regenerative microchannel neural interface for recording from and stimulating peripheral axons *in vivo J. Neural Eng.* **9** 016010

[4] Lacour S P, Atta R, FitzGerald J J, Blamire M, Tarte E and Fawcett J 2008 Polyimide micro-channel arrays for peripheral nerve regenerative implants *Sensors Actuators Phys.* **147** 456–63

[5] Lacour S P, Fitzgerald J J, Lago N, Tarte E, McMahon S and Fawcett J 2009 Long micro-channel electrode arrays: a novel type of regenerative peripheral nerve interface *IEEE Trans. Neural Syst. Rehabil. Eng. Publ. IEEE Eng. Med. Biol. Soc.* **17** 454–60

[6] Kim B, Reyes A, Garza B and Choi Y 2015 A microchannel neural interface with embedded microwires targeting the peripheral nervous system *Microsyst. Technol.* **21** 1551–7

[7] Barrett R, Benmerah S, Frommhold A and Tarte E 2013 Spiral peripheral nerve interface; updated fabrication process of the regenerative implant *2013 35th Annual Int. Conf. IEEE Engineering in Medicine and Biology Society (EMBC)* pp 771–4

[8] Barrett R 2014 Novel processing routes for neural interfaces *PhD Thesis* University of Birmingham

[9] Srinivasan A *et al* 2015 Microchannel-based regenerative scaffold for chronic peripheral nerve interfacing in amputees *Biomaterials* **41** 151–65

[10] Delivopoulos E, Minev I and Lacour S P 2011 Evaluation of negative photo-patternable PDMS for the encapsulation of neural electrodes *2011 5th Int. IEEE/EMBS Conf. on Neural Engineering (NER)* pp 490–4

[11] Delivopoulos E, Chew D J, Minev I R, Fawcett J W and Lacour S P 2012 Concurrent recordings of bladder afferents from multiple nerves using a microfabricated PDMS microchannel electrode array *Lab Chip* **12** 2540–51

[12] Musick K M, Rigosa J, Narasimhan S, Wurth S, Capogrosso M, Chew D J, Fawcett J W, Micera S and Lacour S P 2015 Chronic multichannel neural recordings from soft regenerative microchannel electrodes during gait *Sci. Rep.* **5** 14363

[13] Chew D J *et al* 2013 A microchannel neuroprosthesis for bladder control after spinal cord injury in rat *Sci. Transl. Med.* **5** 210ra155

[14] Starobin J M, Gilani S and Aravamudhan S 2014 Application of micro-/nanotechnology in the design and control of neural interfaces *Nanoscience and Nanoengineering* (Boca Raton, FL: CRC Press) pp 51–66

[15] Starobin J M, Varadarajan V and Aravamudhan S 2011 High-density peripheral nerve resonant stimulation system *Proc. BMES Biomedical Engineering Society Annual Meeting (Hartford, Conneticut, USA)*

[16] FitzGerald J J, Lacour S P and Fawcett J W 2008 Recording with microchannel electrodes in a noisy environment *Conf. Proc. Annual Int. Conf. IEEE Engineering in Medicine Biology Society*vol 2008 pp 34–7

[17] Schuettler M, Stiess S, King B V and Suaning G J 2005 Fabrication of implantable microelectrode arrays by laser cutting of silicone rubber and platinum foil *J. Neural Eng.* **2** S121–8

[18] Suaning G J, Schuettler M, Ordonez J S and Lovell N H 2007 Fabrication of multi-layer, high-density micro-electrode arrays for neural stimulation and bio-signal recording *3rd Int. IEEE/EMBS Conf. on Neural Engineering, 2007, CNE'07* pp 5–8

[19] Schuettler M, Schroeer S, Ordonez J S and Stieglitz T 2011 Laser-fabrication of peripheral nerve cuff electrodes with integrated microfluidic channels *2011 5th Int. IEEE/EMBS Conf. on Neural Engineering (NER)* pp 245–8

[20] Fiedler E, Schuettler M, Henle C, Zengerle R and Stieglitz T 2009 Integration of Microfluidic Channels into Laser-Fabricated Neural Electrode Arrays *4th European Conf. Int. Federation for Medical and Biological Engineering IFMBE Proc.* vol 22 ed J V Sloten *et al* (Berlin: Springer) pp 2431–4

[21] Di Scipio F, Raimondo S, Tos P and Geuna S 2008 A simple protocol for paraffin-embedded myelin sheath staining with osmium tetroxide for light microscope observation *Microsc. Res. Tech.* **71** 497–502

[22] Dodds C W D, Schuettler M, Guenther T, Lovell N H and Suaning G J 2011 Advancements in electrode design and laser techniques for fabricating micro-electrode arrays as part of a retinal prosthesis *2011 Annual Int. Conf. IEEE Engineering in Medicine and Biology Society, EMBC* pp 636–9

[23] Hoffman-Kim D, Mitchel J A and Bellamkonda R V 2010 Topography, cell response, and nerve regeneration *Annu. Rev. Biomed. Eng.* **12** 203–31

[24] Bilston L E 2011 *Neural Tissue Biomechanics* (Berlin: Springer) (doi:10.1007/978-3-642-13890-4)

[25] Schuettler M, Pfau D, Ordonez J S, Henle C, Woias P and Stieglitz T 2009 Stretchable tracks for laser-machined neural electrode arrays *Annual Int. Conf. IEEE Engineering in Medicine and Biology Society, 2009, EMBC 2009* pp 1612–5

[26] Johnston I D, McCluskey D K, Tan C K L and Tracey M C 2014 Mechanical characterization of bulk Sylgard 184 for microfluidics and microengineering *J. Micromech. Microeng.* **24** 035017

[27] Meredith D O, Eschbach L, Wood M A, Riehle M O, Curtis A S G and Richards R G 2005 Human fibroblast reactions to standard and electropolished titanium and Ti–6Al–7Nb, and electropolished stainless steel *J. Biomed. Mater. Res.* A **75A** 541–55

[28] Green R A, Toor H, Dodds C and Lovell N H 2012 Variation in Performance of platinum electrodes with size and surface roughness *Sens. Mater.* **24** 165–80

[29] Green R A, Matteucci P B, Dodds C W D, Palmer J, Dueck W F, Hassarati R T, Byrnes-Preston P J, Lovell N H and Suaning G J 2014 Laser patterning of platinum electrodes for safe neurostimulation *J. Neural Eng.* **11** 056017

[30] Husarik D B, Saupe N, Pfirrmann C W A, Jost B, Hodler J and Zanetti M 2009 Elbow nerves: MR findings in 60 asymptomatic subjects—normal anatomy, variants, and pitfalls *Radiology* **252** 148–56

[31] Gore R K, Choi Y, Bellamkonda R and English A 2015 Functional recordings from awake, behaving rodents through a microchannel based regenerative neural interface *J. Neural Eng.* **12** 016017

[32] Stieglitz T, Beutel H and Meyer J-U 2000 'Microflex'—a new assembling technique for interconnects *J. Intell. Mater. Syst. Struct.* **11** 417–25

[33] Giagka V, Vanhoestenberghe A, Donaldson N and Demosthenous A 2014 Evaluation and optimization of the mechanical strength of bonds between metal foil and aluminium pads on thin ASICs using gold ball studs as micro-rivets *Electronics System-Integration Technology Conference (ESTC) 2014* pp 1–5

[34] Schuettler M, Henle C, Ordonez J S, Meier W, Guenther T and Stieglitz T 2008 Interconnection technologies for laser-patterned electrode arrays *Conf. Proc. Annu. Int. Conf. IEEE Engineering in Medicine and Biology Society*vol 2008 pp 3212–5

[35] Vanhoestenberghe A, Musick K M, Lacour S P and Donaldson N 2012 An interconnection method for ultra-compliant electrodes *17th Annual Int. FES Society Conf.* (Banff, Alberta, Canada: International Functional Electrical Stimulation Society)